

A General Analysis of Single IP₃ Receptors Modulated by Cytosolic Ca²⁺ and IP₃

Chen Jia^{1,*} Yihan Li¹ Minping Qian^{1,2}

¹School of Mathematical Sciences, Peking University, Beijing 100871, China

²Center for Theoretical Biology, Peking University, Beijing 100871, China

Abstract In this report, we remove the constraint of detailed balance and give a general discussion of the modulation of cytosolic Ca²⁺ and IP₃ on the IP₃R channel. By introducing the circulation decomposition theorem in stochastic process, the gating mechanism of single IP₃R is neatly analyzed. Some remarkable differences are found to distinguish between equilibrium and non-equilibrium dynamics. Evidence is given to show that detailed balance is violated to some extent in the IP₃R channel. Comparison of surface fittings between equilibrium and non-equilibrium models reveals that the latter model excels evidently. It is emphasized that these interesting phenomena in the non-equilibrium dynamics, present a more comprehensive view of the channel behavior.

1 Introduction

The inositol 1,4,5-trisphosphate receptor (IP₃R), which plays a crucial role in calcium dynamics, is a channel located in the endoplasmic reticulum (ER) that releases Ca²⁺ ions [1, 2, 3]. Structurally, the IP₃R is a large (~30nm diameter) homomeric tetramer of four subunits forming a single ion-conducting channel [4]. The gating of IP₃R channels requires the binding of the second messenger inositol 1,4,5-trisphosphate (IP₃) [1, 3]. Subsequent release of Ca²⁺ ions from the ER can further modulate gating of the IP₃R channel. Small elevations of cytosolic [Ca²⁺] promote channel opening whereas higher elevations result in inactivation [5, 6, 7]. This positive and negative Ca²⁺ feedback effect underlies a process of Calcium-induced Calcium release (CICR) which can result in oscillations and waves of [Ca²⁺] [1, 3].

Many deterministic and stochastic IP₃R models have been developed to explain and understand experimental data [8, 9, 10, 11, 12]. As one of the early binding models, the De Young-Keizer model is most widely applied to describe experimental data obtained from IP₃R reconstructed in bilayers membrane [8]. However, there are significant differences in behavior of the reconstituted IP₃R versus that of IP₃R in their native environment of the nuclear envelope [3]. In order to describe IP₃R data obtained on nuclei membrane, the Mak-McBride-Foskett allosteric model [11] and the Baran allosteric model [12] were proposed. To bridge these two levels of experimental data, Shuai, Pearson et al. developed a dynamic IP₃R model in *Xenopus* oocytes to predict the behavior of individual and clustered channels [3].

*Corresponding author. Email: jcbeyboy@126.com

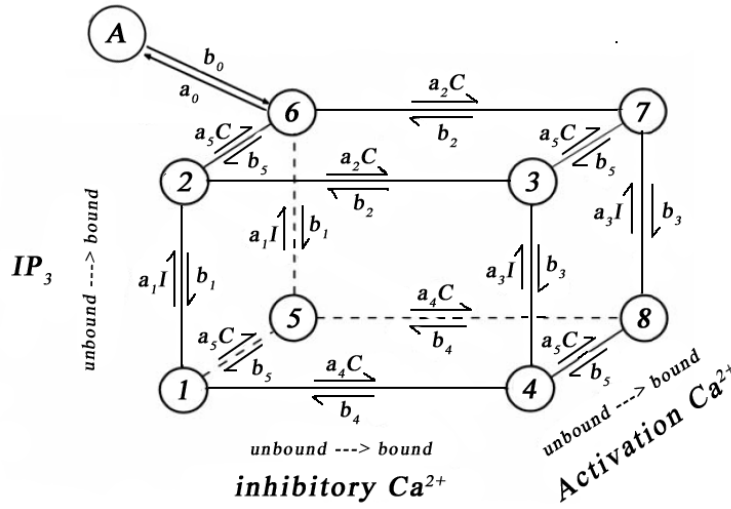


Figure 1: Schematic picture of the IP₃R model of a single subunit

In the Shuai-Pearson model, detailed balance was imposed for mathematical simplification. However, evidence shows that the IP₃R channel violates detailed balance to a large extent. Thus, there is still a lack of general discussion of how single IP₃R channels are modulated by cytosolic Ca²⁺ and IP₃. Our aim is to remove the constraint of detailed balance and investigate differences between equilibrium and non-equilibrium dynamics. Fortunately, by introducing the circulation decomposition theorem in stochastic process, the channel behavior modulated by cytosolic Ca²⁺ and IP₃ can be neatly analyzed [13].

2 Model

2.1 General Description

In the Shuai-Person IP₃R model, each channel consists of four independent and identical subunits. For each subunit, there are three independent binding sites — an IP₃ binding site, an activating Ca²⁺ binding site and an inhibitory Ca²⁺ binding site. Eight states are introduced to describe the subunit dynamics according to whether three binding sites are occupied or not. The model further includes a conformational change whereby a subunit in state 6 (one IP₃ and one activating Ca²⁺ bound) is ‘inactive’, and must transfer to an ‘active’ state before it can contribute to channel opening. These eight states and an extra ‘active’ state constitute a total of nine states for each subunit (see Fig. 1). The channel opens when three or all of the four independent subunits are at the ‘active’ state.

Mathematically, the subunit dynamics described in Fig. 1 can be modeled as a continuous time Markov chain X_t with a finite state space $\mathcal{S} = \{1, 2, 3, 4, 5, 6, 7, 8, A\}$. The transition rates of the Markov chain can be readily read out from Fig. 1, where a_i and b_i are rate constants, I and C represent concentrations of IP₃ and Ca²⁺ respectively. In this report, we remove the constraint of detailed balance and assume that the system achieves a non-equilibrium steady state. In the following text, it is equivalent to say that the ion

channel satisfies (violates) detailed balance and the ion channel is in the equilibrium (non-equilibrium) case.

2.2 Basic Computations

We need first to calculate the invariant (steady) probability distribution of the Markov chain X_t . Under the constraint of detailed balance, the results can be easily acquired. In the non-equilibrium case, however, we introduced the circulation decomposition theorem [13] into solving this problem.

Let $\mu = (\mu_1, \mu_2, \mu_3, \mu_4, \mu_5, \mu_6, \mu_7, \mu_8, \mu_A)$ be the invariant distribution of the Markov chain X_t . Since state A can only transit to state 6, the probability fluxes between state 6 and state A are identical, that is

$$a_0\mu_6 = b_0\mu_A. \quad (1)$$

This implies that transitions between state 6 and state A do not affect transitions among other states. To clarify, we consider a Markov chain \tilde{X}_t , derived from X_t but restricted to states $\{1, 2, \dots, 8\}$ (without state A). It follows from (1) that $(\mu_1, \mu_2, \mu_3, \mu_4, \mu_5, \mu_6, \mu_7, \mu_8)$ is an invariant measure of \tilde{X}_t . Thus the invariant distribution of \tilde{X}_t is

$$\left(\frac{\mu_1}{1 - \mu_A}, \frac{\mu_2}{1 - \mu_A}, \dots, \frac{\mu_8}{1 - \mu_A} \right).$$

For further analysis, we divide the state space into two parts and denote the subspace $\{5, 6, 7, 8\}$ by \mathcal{S}_1 , and the subspace $\{1, 2, 3, 4\}$ by \mathcal{S}_2 . We also decompose \tilde{X}_t into the coupling of two Markov chains. Specifically, we put $\tilde{X}_t = (Y_t, Z_t)$, where

$$Y_t = \begin{cases} 0, & \text{if } X_t \in \mathcal{S}_2, \\ 1, & \text{if } X_t \in \mathcal{S}_1, \end{cases}$$

and

$$Z_t = \begin{cases} 1, & \text{if } X_t \in \{1, 5\}, \\ 2, & \text{if } X_t \in \{2, 6\}, \\ 3, & \text{if } X_t \in \{3, 7\}, \\ 4, & \text{if } X_t \in \{4, 8\}. \end{cases}$$

Note that the corresponding transition rates among state pairs 1 and 5, 2 and 6, 3 and 7, 4 and 8 are identical. Moreover, the corresponding transition rates in \mathcal{S}_1 and \mathcal{S}_2 are also the same (see Fig. 1). These particular relationships between transition rates implies that Y_t and Z_t are **independent** Markov chains under the above decomposition. Hence the invariant distribution of \tilde{X}_t is the product of the invariant distributions of Y_t and Z_t .

Since Y_t is a two-state Markov chain with transition rates a_5C and b_5 , the invariant distribution of Y_t is $(\frac{b_5}{a_5C+b_5}, \frac{a_5C}{a_5C+b_5})$. This shows that the invariant distribution of \tilde{X}_t satisfies

$$\frac{\mu_i}{1 - \mu_A} = \frac{b_5}{a_5C} \frac{\mu_{i+4}}{1 - \mu_A}.$$

Hence, the invariant distribution of X_t satisfies

$$a_5C\mu_i = b_5\mu_{i+4} \quad (i = 1, 2, 3, 4). \quad (2)$$

The above equation implies that the corresponding states between \mathcal{S}_1 and \mathcal{S}_2 satisfy detailed balance; net circulations only exist in the two cycles along \mathcal{S}_1 and \mathcal{S}_2 .

Let J be the cycle flux along state 5 \rightarrow state 6 \rightarrow state 7 \rightarrow state 8 \rightarrow state 5. According to the circulation decomposition theorem, we have the following set of equations:

$$\begin{cases} J = a_1 I \mu_5 - b_1 \mu_6, \\ J = a_2 C \mu_6 - b_2 \mu_7, \\ J = b_3 \mu_7 - a_3 I \mu_8, \\ J = b_4 \mu_8 - a_4 C \mu_5. \end{cases} \quad (3)$$

In addition, the normalization condition leads to $\sum_{i \in S} \mu_i = 1$.

By (3), we use μ_6 and J to represent other steady probabilities and obtain

$$\begin{cases} \mu_5 = \frac{k_1}{I} \mu_6 + \frac{1}{a_1 I} J, \\ \mu_7 = \frac{C}{k_2} \mu_6 - \frac{1}{b_2} J, \\ \mu_8 = \frac{k_3 C}{k_2 I} \mu_6 - \left(\frac{k_3}{b_2 I} + \frac{1}{a_3 I} \right) J. \end{cases} \quad (4)$$

Moreover, the relationship between μ_6 and J are included in the following two equations:

$$\begin{cases} J = \frac{KC}{D_1} \mu_6, \\ \mu_6 = \frac{nI}{D_3} + \frac{D_2}{D_3} J, \end{cases} \quad (5)$$

where $k_i = \frac{b_i}{a_i}$ ($i = 0, 1, \dots, 5$), $K = \frac{k_3}{k_2} - \frac{k_1}{k_4}$, $n = \frac{C}{C+k_5}$ and

$$\begin{aligned} D_1 &= \frac{I}{b_4} + \frac{C}{a_1 k_4} + \frac{k_3}{b_2} + \frac{1}{a_3} = n_1 I + n_2 = m_1 C + m_2, \\ D_2 &= \frac{I}{b_2} + \frac{k_3}{b_2} + \frac{1}{a_3} - \frac{1}{a_1} = n_3 I + n_4, \\ D_3 &= \left(1 + \frac{C}{k_2} + \frac{C}{(C+k_5)k_0} \right) I + \left(k_1 + \frac{k_3 C}{k_2} \right) = n_5 I + n_6. \end{aligned} \quad (6)$$

Note that the sign of D_2 is indeterminate, while D_1 and D_3 are always positive. (5) shows that the sign of J the same as the sign of K . Especially, $J = 0$ (detailed balance condition) is equivalent to $K = 0$ ($k_1 k_2 = k_3 k_4$).

3 Role of IP₃ and Ca²⁺ as modulators

With the above model, we now discuss the modulation of [IP₃] and [Ca²⁺] on μ_6 and these modulations may differ in equilibrium and non-equilibrium cases.

Recall that

$$\mu_6 = \frac{nI}{D_3} + \frac{D_2}{D_3} J = \mu_6^{(1)} + \mu_6^{(2)}.$$

We can see that the steady probability μ_6 consists of two parts. When the system is in equilibrium ($J = 0$), only the first part remains. This indicates that the first part (denoted by $\mu_6^{(1)}$) represents the contribution of the equilibrium factor, while the second part (denoted by $\mu_6^{(2)}$) represents the contribution of the non-equilibrium factor.

3.1 Modulation of IP₃ on μ_6

In this section, we take the overall effect μ_6 , the equilibrium factor $\mu_6^{(1)}$ and the non-equilibrium factor $\mu_6^{(2)}$ as functions of I .

3.1.1 Equilibrium and Non-equilibrium factor

According to (6), we obtain $\mu_6^{(1)}(I) = \frac{nI}{n_5I + n_6}$. It is clear that the equilibrium factor $\mu_6^{(1)}$ is a monotonically increasing function of I . Hence when the system is in equilibrium, the overall effect $\mu_6 (= \mu_6^{(1)})$ will never decrease as I increases.

Still referring to (6), we have

$$\mu_6^{(2)}(I) = \frac{D_2}{D_3}J = \frac{n_3I + n_4}{n_5I + n_6}J.$$

By expressing J in terms of I , we have $\mu_6^{(2)}(0) = 0$ and $\lim_{I \rightarrow \infty} \mu_6^{(2)}(I) = 0$. The following discussion illustrates that there are four different situations, according to the monotonicity of $\mu_6^{(2)}$ with respect to I .

- $n_4 > 0, K > 0$

As mentioned earlier, the variable D_3 is positive. $D_2 = n_3I + n_4$ is positive when $n_4 > 0$ and the cycle flux J is positive when $K > 0$. Thus in this situation, $\mu_6^{(2)}$ is always positive (see the green line in Fig. 2a.)

- $n_4 > 0, K < 0$

$n_4 > 0$ and $K < 0$ lead to $D_2 = n_3I + n_4 > 0$ and $J < 0$. Hence in this situation, $\mu_6^{(2)}$ is always negative (see Fig. 2b).

- $n_4 < 0, K > 0$

$K > 0$ implies that $J > 0$. However, the trend of D_2 is rather complicated. Since $n_4 < 0$ and $n_3 > 0$, a change will occur in the sign of $D_2 = n_3I + n_4$ as I increases. Hence in this situation, $\mu_6^{(2)}$ will be first negative then positive as I increase (see Fig. 2c).

- $n_4 < 0, K < 0$

In this situation, we have $J < 0$. Similar reason shows that $\mu_6^{(2)}$ is first positive then negative as I increases (see Fig. 2d).

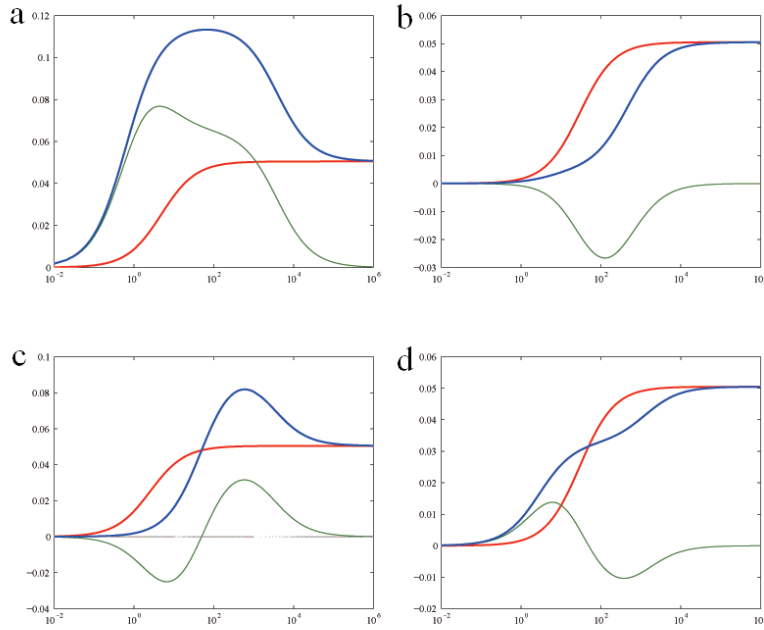


Figure 2: Plots of the overall effect μ_6 (blue), the equilibrium factor $\mu_6^{(1)}$ (red) and the non-equilibrium factor $\mu_6^{(2)}$ (green) versus $[IP_3]$. **a**, $n_4 > 0, K > 0$. **b**, $n_4 > 0, K < 0$. **c**, $n_4 < 0, K > 0$. **d**, $n_4 < 0, K < 0$.

3.1.2 Overall effect

By (5), basic calculation shows that

$$\mu_6 = \frac{D_1 n I}{D_1 D_3 - D_2 K C}.$$

Since D_1 , D_2 and D_3 are all linear functions of I , the overall effect μ_6 takes the general form of

$$\mu_6(I) = \frac{x_1 I^2 + x_2 I}{y_1 I^2 + y_2 I + y_3},$$

where parameters x_1 , x_2 , y_1 and y_3 are all positive, but the sign of parameter y_2 is uncertain.

In order to clarify the monotonicity of the function $\mu_6(I)$, we calculate the derivative:

$$\mu_6'(I) = \frac{(x_1 y_2 - x_2 y_1) I^2 + 2x_1 y_3 I + x_2 y_3}{(y_1 I^2 + y_2 I + y_3)^2}.$$

If $x_1 y_2 - x_2 y_1 > 0$, $\mu_6'(I)$ is always positive and thus μ_6 is a monotonically increasing function of I . If $x_1 y_2 - x_2 y_1 < 0$, $\mu_6'(I)$ is first negative then positive as I increases; hence

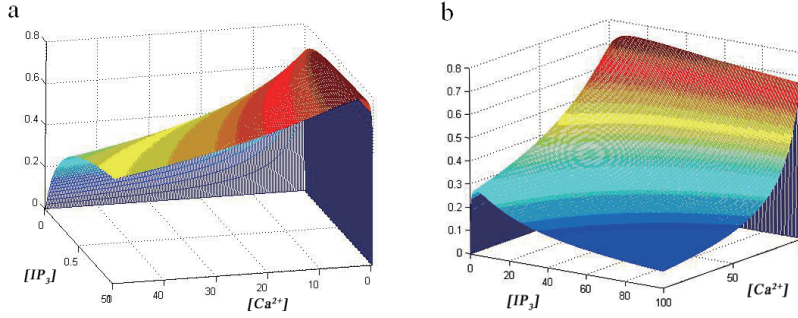


Figure 3: Surfaces of overall effect μ_6 versus $[\text{IP}_3]$ and $[\text{Ca}^{2+}]$. **a**, $x_1y_2 - x_2y_1 > 0$. **b**, $x_1y_2 - x_2y_1 < 0$.

μ_6 first increases to its maximum then decreases as I increases (see Fig. 3 and the blue line in Fig. 2).

3.2 Modulation of Ca²⁺ on μ_6

In this section, we take the overall effect μ_6 , the equilibrium factor $\mu_6^{(1)}$ and the non-equilibrium factor $\mu_6^{(2)}$ as functions of C . We omit the proofs and conclude that μ_6 is a bell-shaped function of C regardless of equilibrium or non-equilibrium dynamics. Although the overall trend of C on μ_6 does not change when the non-equilibrium factor is added, we are still concerned about how μ_6 will be influenced by the cycle flux J .

Recall that

$$\mu_6^{(2)}(C) = \frac{D_2 J}{D_3}.$$

Basic calculation shows that $\mu_6^{(2)}(0) = 0$ and $\lim_{C \rightarrow \infty} \mu_6^{(2)}(C) = 0$. Moreover, the modulation of C on $\mu_6^{(2)}$ presents simpler properties than that of IP₃. When $D_2K > 0$, $\mu_6^{(2)}$ is always positive (see the green curve in Fig. 4a). When $D_2K < 0$, however, $\mu_6^{(2)}$ is always negative (see the green curve in Fig. 4b).

As illustrated in Fig. 4, when the non-equilibrium factor is positive, it raises the value of μ_6 and makes the modulating range of $[\text{Ca}^{2+}]$ on μ_6 wider; when the non-equilibrium factor is negative, it drops the value of μ_6 and makes the modulating range of $[\text{Ca}^{2+}]$ on μ_6 narrower.

4 Further discussion of channel behavior

The open probability, mean open and close times for the IP₃R channel are important observable quantities that reveal the gating mechanism. In this section, we discuss the modulation of $[\text{IP}_3]$ and $[\text{Ca}^{2+}]$ on those quantities. Moreover, by introducing the utilization effect of IP₃, the modulating effect of IP₃ are further analyzed.

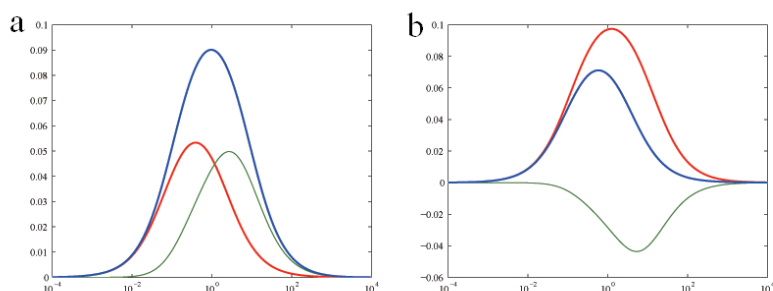


Figure 4: Plots of the overall effect μ_6 (blue), the equilibrium factor $\mu_6^{(1)}$ (red) and the non-equilibrium factor $\mu_6^{(2)}$ (green) versus $[\text{Ca}^{2+}]$. **a**, $D_2K > 0$. **b**, $D_2K < 0$.

4.1 Open probability

As is described above, the channel is open when three or all of the four independent subunits are in the ‘active’ state (state A). It is not hard to see that the open probability for an IP₃R channel is given by

$$P_o = \mu_A^4 + 4\mu_A^3(1 - \mu_A),$$

where μ_A is the steady probability of state A of each subunit. Since P_o monotonically increases as μ_A increases from 0 to 1, the modulating effects of $[\text{IP}_3]$ and $[\text{Ca}^{2+}]$ on P_o are almost the same as those on μ_A (or μ_6).

4.2 Mean open and close times

In Ref. [3], expressions of the mean open and close times are given. However, we do not find those results clear and evident. In fact, from the perspective of Markov chains, those results can be strictly stated and proved.

In the appendix, a mathematical theorem is given to calculate the mean open and close times. The theorem shows that if we partition the state space of a continuous time Markov Chain into two subspaces, which we denote by the ‘open’ subspace Λ_1 and the ‘closed’ subspace Λ_2 , then the mean duration in Λ_1 (Λ_2) is the quotient of the steady probability in Λ_1 (Λ_2) over the total probability flux from Λ_1 (Λ_2) to Λ_2 (Λ_1).

With the above model, an IP₃R channel can be modeled as the coupling of four i.i.d. Markov Chains each of which represents a subunit. The ‘open’ subspace of the IP₃R channel consists of two parts: (i) only three subunits are in the ‘active’ state (denoted by S_3); (ii) all the four subunits are in the ‘active’ state (denoted by S_4).

It is clear that the steady probability in S_3 has the form of $p_3 = 4\mu_A^3(1 - \mu_A)$ while the steady probability in S_4 takes the form of $p_4 = \mu_A^4$. Note that only S_3 can directly transit to the ‘closed’ subspace by any one of the three subunits transiting from state A to state B with rate b_0 , while S_4 must first transit to the S_3 before transiting to the ‘closed’ subspace. Hence the total probability flux from the ‘open’ subspace to the ‘closed’ subspace is $p_3 \cdot 3b_0$.

Let τ_o and τ_c be the mean open and close times respectively. According to the theorem described above, we obtain

$$\tau_o = \frac{p_3 + p_4}{p_3 \cdot 3b_0} = \frac{1}{3b_0} \left(1 + \frac{p_4}{p_3} \right) = \frac{1}{3b_0} \left(1 + \frac{1}{\frac{4}{\mu_A} - 4} \right).$$

and

$$\tau_c = \frac{1 - (p_3 + p_4)}{p_3 \cdot 3b_0} = \frac{1}{3b_0} \cdot \frac{1 - 4\mu_A^3(1 - \mu_A) - \mu_A^4}{4\mu_A^3(1 - \mu_A)}.$$

It is not hard to see that τ_o and τ_c are monotonically increasing and decreasing functions of μ_A respectively. Hence [Ca²⁺] and [IP₃] modulate τ_o in the same way as they do μ_6 , while the modulating effect of [Ca²⁺] and [IP₃] on τ_c are contrary to those on μ_6 .

4.3 Utilization effect of IP₃

IP₃ plays a central role in the channel opening, not only because the binding of the messenger IP₃ itself is indispensable, but it also influences the binding of both activating and inhibitory Ca²⁺ (see Fig. 1). Therefore, further analysis on how IP₃ is utilized is needed.

As in Fig. 1, states in the upper layer of the cube are bound with IP₃, while states in the lower layer are not. Note that only the transition rates from the lower layer to the upper layer are related to [IP₃]. Hence the ratio of the steady probability in the upper layer to that of the lower layer reflects the utilization of [IP₃].

It is reasonable to define the quantity

$$R = \frac{\mu_2 + \mu_3 + \mu_6 + \mu_7}{\mu_1 + \mu_4 + \mu_5 + \mu_8}$$

as the utilization effect of IP₃. Since the dependence of the utilization effect R on [IP₃] is concerned, we take R as a function of I . It follows from (2) and (4) that

$$R(I) = \frac{l_1\mu_6 - \frac{1}{b_2}J}{l_3\mu_6 - \left(\frac{1}{a_3} + \frac{k_3}{b_2} - \frac{1}{a_1}\right)J}I,$$

where l_1 and l_3 are coefficients independent of I .

When the system is in equilibrium ($J = 0$), we have $R(I) = \frac{l_1}{l_3}I$. That is to say, when detailed balance is satisfied, the utilization effect is positively proportional to [IP₃].

When the system is in non-equilibrium, by (5) and (6), we obtain

$$R(I) = \frac{l_1n_1I + (l_1n_2 - l_2)}{l_3n_1I + (l_3n_2 - l_4)}I,$$

where l_2 and l_4 are coefficients independent of I . It is clear that $R(I)$ monotonically increases with I . Furthermore, we observe that when I is very small, $R(I)$ approximately equals to $\frac{l_1n_2 - l_2}{l_3n_2 - l_4}I$; when I is very large, $R(I)$ approximately equals to $\frac{l_1}{l_3}I$. The increasing trend of $R(I)$ may speed up or slow down as I increases, depending on whether $\frac{l_1}{l_3}$ or $\frac{l_1n_2 - l_2}{l_3n_2 - l_4}$ is larger (see Fig. 5).

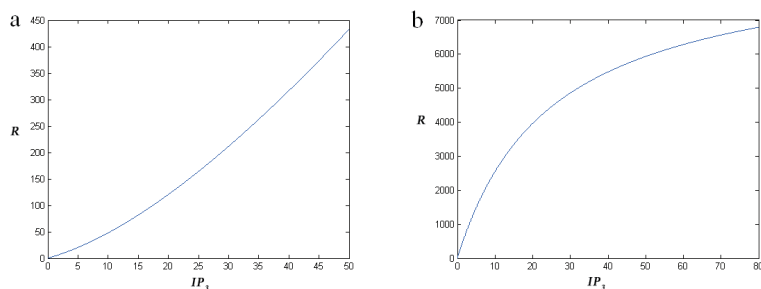


Figure 5: Plots of the utilization effect R versus $[IP_3]$. **a**, Increasing trend speeds up. **b**, Increasing trend slows down.

Table 1: Part of the patch-clamp data

$[IP_3]$ (μM)	$[Ca^{2+}]$ (μM)	P_o
0.033	32.5	0.0503
0.1	32.5	0.8252
10	32.5	0.6917

The above results show another essential difference between equilibrium and non-equilibrium cases. In the equilibrium dynamics, the utilization effect of IP_3 increases at a constant rate as $[IP_3]$ increases. In the non-equilibrium dynamics, however, the increasing rate of the utilization effect does not remain a constant. Roughly speaking, compared to the equilibrium dynamics, the utilization effect of IP_3 tends to be more sensitive to the change of $[IP_3]$ in non-equilibrium.

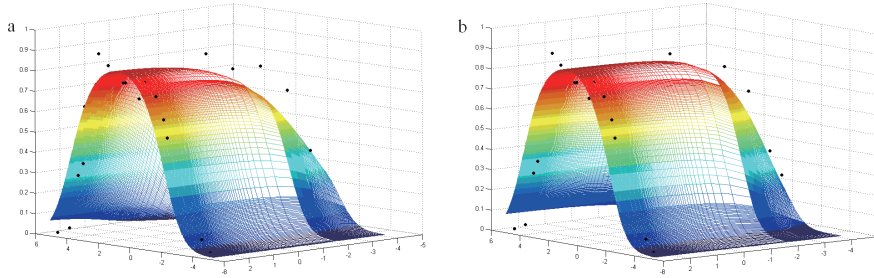
5 Violation of Detailed Balance

The *Xenopus* oocyte provides a favorable cell system with which to investigate the channel behavior by virtue of the wealth of steady-state experimental data obtained from patch-clamped oocyte nuclear IP_3R . [3, 14, 15, 16, 17, 18]. Patch-clamped experimental data shows that when $[Ca^{2+}]$ is fixed at $32.5\mu\text{M}$, the open probability P_o first increases from 0.0503 to 0.8252 when $[IP_3]$ increases from $0.033\mu\text{M}$ to $0.1\mu\text{M}$, then decreases to 0.6917 when $[IP_3]$ increases to its saturated concentration of $10\mu\text{M}$ (see Tab. 1). This phenomenon can never occur under the constraint of detailed balance. The above evidence implies that the IP_3R channel, at least to some extent, violates detailed balance.

In Tab. 2, rate constants are estimated on the basis of the optimal fit to the patch-clamped data in equilibrium and non-equilibrium cases respectively. It is worth noting that the estimated values in the two cases differ much. Those estimated without the constraint of detail balance satisfy $K = \frac{k_3}{k_2} - \frac{k_1}{k_4} < 0$. The deviation of K from 0 implies the violation of detailed balance. Moreover, the comparison of surface fittings show that the non-equilibrium dynamics excels evidently when the $[IP_3]$ is low (see Fig. 6).

Table 2: Comparison of the transition rates in equilibrium and non-equilibrium cases

	Parameter	Value in equilibrium	Value in non-equilibrium
Conformational Change	a_0	540 s^{-1}	540 s^{-1}
	b_0	80 s^{-1}	77.544 s^{-1}
IP ₃ Binding Site	a_1	$60 \mu\text{M}^{-1}\text{s}^{-1}$	$62.3695 \mu\text{M}^{-1}\text{s}^{-1}$
	k_1	$0.0036 \mu\text{M}$	$0.0205 \mu\text{M}$
	a_3	$5.0 \mu\text{M}^{-1}\text{s}^{-1}$	$3.4132 \mu\text{M}^{-1}\text{s}^{-1}$
	k_3	$0.8 \mu\text{M}$	$0.0129 \mu\text{M}$
Activating Ca ²⁺ Binding Site	a_5	$150 \mu\text{M}^{-1}\text{s}^{-1}$	$150 \mu\text{M}^{-1}\text{s}^{-1}$
	k_5	$0.8 \mu\text{M}$	$0.8881 \mu\text{M}$
Inhibitory Ca ²⁺ Binding Site	a_2	$0.2 \mu\text{M}^{-1}\text{s}^{-1}$	$0.0562 \mu\text{M}^{-1}\text{s}^{-1}$
	k_2	$16 \mu\text{M}$	$16.4555 \mu\text{M}$
	a_4	$0.5 \mu\text{M}^{-1}\text{s}^{-1}$	$0.0715 \mu\text{M}^{-1}\text{s}^{-1}$
	k_4	$0.072 \mu\text{M}$	$0.0001 \mu\text{M}$


Figure 6: Surface Fittings of the open probability versus the logarithm of $[\text{Ca}^{2+}]$ and $[\text{IP}_3]$. **a**, Equilibrium Case. **b**, Non-equilibrium Case.

6 Summary

The gating mechanism of a single IP₃R channel plays a basic role in understanding the complex dynamic behavior of Ca²⁺ signaling [1, 3, 19, 20, 21]. In this report, a general discussion is given to analyze the modulation of $[\text{Ca}^{2+}]$ and $[\text{IP}_3]$ on single IP₃R channels.

In view of the inconsistency between patch-clamp experimental data and the equilibrium model, we take the non-equilibrium factor into account. By introducing the circulation decomposition theorem in stochastic process into this problem, the channel behavior modulated by cytosolic Ca²⁺ and IP₃ can be neatly analyzed.

Topics and quantities discussed in this paper include the open probability, the mean open and close durations, and the utilization effect of IP₃. More important, Some essential and remarkable differences are found to distinguish between equilibrium and non-equilibrium cases.

(i) In the non-equilibrium case, the open probability and mean open time may not monotonically increase as $[\text{IP}_3]$ increases. $[\text{IP}_3]$ must be controlled within a certain range to

maintain high open probability and mean open time.

(ii) The open probability and mean open time are always bell-shaped functions of $[Ca^{2+}]$. Compared to the equilibrium case, the non-equilibrium factor will result in wider or narrower modulating range of $[Ca^{2+}]$ on both quantities.

(iii) In the non-equilibrium dynamics, the increasing trend of the utilization effect of $[IP_3]$ may speed up or slow down as $[IP_3]$ increases; the utilization effect of IP_3 tends to be more sensitive to the change of $[IP_3]$ than the equilibrium dynamics.

All these differences reveal limitations of presuming detailed balance and give us a more comprehensive view of the behavior of the single IP_3R . Further analysis is needed for deeper insights into the channel behavior in the non-equilibrium dynamics.

7 Appendix

Theorem 1.

Let $\{X_t, t \geq 0\}$ be a continuous time Markov chain on state space S , with generator matrix $Q = (q_{ij})$. S_1 and S_2 are subspaces of S satisfying

$$S = S_1 \cup S_2, \quad S_1 \cap S_2 = \emptyset, \quad S_1, S_2 \neq \emptyset.$$

Suppose the invariant distribution $\mu = \{\mu_i : i \in S\}$ exists, then the mean duration in S_1 (denoted by ξ) takes the form of

$$\xi = \frac{\sum_{i \in S_1} \mu_i}{\sum_{i \in S_1} \sum_{j \in S_2} \mu_i q_{ij}}.$$

Proof: By definition, $\sum_{i \in S_1} \mu_i$ represents the mean time staying in S_1 in one time unit. Thus $(\sum_{i \in S_1} \mu_i)/\xi$ represents the mean number of times of leaving S_1 in one time unit. It is not hard to see that

$$\frac{\sum_{i \in S_1} \mu_i}{\xi} = \sum_{i \in S_1} \sum_{j \in S_2} N_{ij},$$

where N_{ij} represents the mean number of times of transition from state $i \in S_1$ to state $j \in S_2$ in one time unit.

It is clear that the mean number of times of leaving state i in one time unit is $1/E_i\sigma_i$, where $E_i\sigma_i$ denotes the mean time it takes a Markov chain starting from state i to return to state i . Hence, we have $N_{ij} = \frac{1}{E_i\sigma_i} p_{ij}$, where $p_{ij} = \frac{q_{ij}}{q_i}$ represents the transition probability from i to j of the imbedded chain.

Ergodic theorem of Markov chains gives that $\mu_i = \frac{1}{q_i E_i \sigma_i}$. Consequently,

$$\frac{\sum_{i \in S_1} \mu_i}{\xi} = \sum_{i \in S_1} \sum_{j \in S_2} \frac{1}{E_i \sigma_i} p_{ij} = \sum_{i \in S_1} \sum_{j \in S_2} \frac{q_{ij}}{q_i E_i \sigma_i} = \sum_{i \in S_1} \sum_{j \in S_2} \mu_i q_{ij},$$

which completes the proof.

References

- [1] Sneyda, J., M. Falckeb. 2005. Models of the Inositol Trisphosphate Receptor. *Progress in Biophysics and Molecular Biology*, Volume 89, Issue 3.

- [2] Christopher P. Fall. 2002. *Computational Cell Biology*. Springer.
- [3] Jianwei Shuai, John E. Pearson, J. Kevin Foskett, Don-On Daniel Mak, Ian Parker. 2007. A kinetic model of single and clustered IP₃ receptors in the absence of Ca²⁺ Feedback *Biophysical Journal*. 107:108795.
- [4] Tayloy, C.W., P. Lipp, and M.D. Bootman. 2000. The versatility and universality of calcium signalling. *Nature Reviews Molecular Cell Biology*. 1:11-21.
- [5] Bezprozvanny, I., J. Watras, and B.E. Ehrlich. 1991. Bell-shaped calcium response curves of Ins(1,4,5)P₃- and calcium-gated channels from endoplasmic reticulum of cerebellum. *Nature*. 351: 751-4.
- [6] Mak, D.O., S. McBride, and J.K. Foskett. 1998. Inositol 1,4,5-trisphosphate activation of inositol trisphosphate receptor Ca²⁺ channel by ligand tuning of Ca²⁺ inhibition. *Proc Natl Acad Sci U S A*. 95: 15821-5.
- [7] Mak, D.O., S. McBride, and J.K. Foskett. 1999. ATP regulation of type 1 inositol 1,4,5-trisphosphate receptor channel gating by allosteric tuning of Ca²⁺ activation. *J. Biol. Chem*. 274:22231-22237.
- [8] De Young, G.W. and J. Keizer. 1992. A single-pool inositol 1,4,5-trisphosphate receptor-based model for agonist-stimulated oscillations in Ca²⁺ concentration. *Proc Natl Acad Sci U S A*. 89: 9895-9.
- [9] Sneyd, J. and J.F. Dufour. 2002. A dynamic model of the type-2 inositol trisphosphate receptor. *Proceedings of the National Academy of Sciences of the United States of America*. 99: 2398-2403.
- [10] Sneyd, J. and M. Falcke. 2005. Models of the inositol trisphosphate receptor. *Progress in Biophysics & Molecular Biology*. 89: 207-245.
- [11] Mak, D.O., S.M. McBride, and J.K. Foskett. 2003. Spontaneous channel activity of the inositol 1,4,5-trisphosphate (InsP₃) receptor (InsP₃R). Application of allosteric modeling to calcium and InsP₃ regulation of InsP₃R single-channel gating. *J Gen Physiol*. 122: 583-603.
- [12] Baran, I. 2003. Integrated luminal and cytosolic aspects of the calcium release control. *Biophysical Journal*. 84:1470-1485.
- [13] Jiang, D.Q., M. Qian, and M.P. Qian. 2004. *Mathematical Theory of Non-equilibrium Steady States*. Springer.
- [14] Mak, D.O. and J.K. Foskett. 1994. Single-channel inositol 1,4,5-trisphosphate receptor currents revealed by patch clamp of isolated *Xenopus* oocyte nuclei. *J Biol Chem*. 269: 29375-8.
- [15] Mak, D.O. and J.K. Foskett. 1997. Single-channel kinetics, inactivation, and spatial distribution of inositol trisphosphate (IP₃) receptors in *Xenopus* oocyte nucleus. *J Gen Physiol*. 109: 571-87.
- [16] Yao, Y., J. Choi, and I. Parker. 1995. Quantal Puffs of Intracellular Ca²⁺ Evoked by Inositol Trisphosphate in *Xenopus* Oocytes. *Journal of Physiology-London*. 482: 533-553.
- [17] Parker, I., Y. Yao, and V. Ilyin. 1996. Fast kinetics of calcium liberation induced in *Xenopus* oocytes by photoreleased inositol trisphosphate. *Biophysical Journal*. 70: 222-237.
- [18] Callamaras, N., J.S. Marchant, X.P. Sun, and I. Parker. 1998. Activation and coordination of InsP₃-mediated elementary Ca²⁺ events during global Ca²⁺ signals in *Xenopus* oocytes. *Journal of Physiology-London*. 509: 81-91.
- [19] Shuai, J.W. and P. Jung. 2002. Stochastic properties of Ca²⁺ release of inositol 1,4,5-trisphosphate receptor clusters. *Biophysical Journal*. 83: 87-97.
- [20] Shuai, J.W. and P. Jung. 2003. Optimal ion channel clustering for intracellular calcium signaling. *Proc Natl Acad Sci U S A*. 100: 506-10.
- [21] Shuai, J.W., H.J. Rose, and I. Parker. 2006. The Number and Spatial Distribution of IP₃ Receptors Underlying Calcium Puffs in *Xenopus* Oocytes. *Biophysical Journal*. 91: 4033-44.